Bioanalytical Sensors

DOI: 10.1002/anie.201006167

Periplasmic Binding Proteins as Optical Modulators of Single-Walled Carbon Nanotube Fluorescence: Amplifying a Nanoscale Actuator**

*Hyeonseok Yoon, Jin-Ho Ahn, Paul W. Barone, Kyungsuk Yum, Richa Sharma, Ardemis A. Boghossian, Jae-Hee Han, and Michael S. Strano**

Periplasmic binding proteins (PBPs) are non-enzymatic receptors in bacteria and play a vital role in transporting small-molecule ligands such as carbohydrates, amino acids, vitamins, and ions.[1] Importantly, most PBPs can adopt two distinct conformations (open and closed forms) which are mediated by the presence of specific ligands. The closed conformation predominates in the presence of the target ligand and accommodates the ligand inside the binding site. This mechanical action of PBPs motivates their use as nanoscale actuators. While PBPs have been incorporated into electrochemical sensors extensively,[2] and used to induce a fluorescence resonance energy transfer response to grafted donor/acceptor fluorophores to their surface,[3] PBPs remain unexplored as direct actuators of nanoscale devices. One of the notable PBPs includes glucose-binding protein (GBP) that is a monomeric protein capable of recognizing glucose (β-D-glucose) with a high affinity. GBP has a bilobate structure of two main domains linked by three peptide segments that act as a hinge. The glucose-binding site is located in the cleft between the two domains.[4] Interestingly, GBP also undergoes a sizable change in conformation upon glucose binding to initiate a signal transduction.[5]

There is interest in modulating single-walled carbon nanotube (SWNT) fluorescence in response to glucose to create a biomedical device that exploits the near infrared (NIR) emission of SWNT, where blood and tissues are most transparent,[6] as discussed previously.[7] In the case of PBPs, and GBP specifically, there has not been an exploration of how such biomechanical proteins can actuate nanoscale devices, for example a fluorescent SWNT. Here, we use GBP to mechanically actuate a fluorescent SWNT, resulting in reversible exciton quenching in response to glucose (Figure 1a). The GBP is covalently conjugated with carboxylated poly(vinyl alcohol)-wrapped SWNTs (cPVA/SWNTs), which leads to allosterically controlled optical transduction in response to glucose. To couple GBP and SWNT, the former was heterologously expressed in *Escherichia coli* (Supporting Information, Figures S1 and S2) and the latter was colloidally dispersed with carboxylated PVA (cPVA). Carboxy groups on the cPVA/SWNT complex were used to attach the protein, through amine coupling to lysine residues on the GBP (Figure S3). These complexes demonstrate a reversible fluorescence quenching in response to glucose, as described below. Figure 1a illustrates the idealized structure of the resulting GBP-PVA/SWNT conjugate. The hypothesis is that the hinge bending action associated with glucose recognition modulates the fluorescence of the SWNT.[8] Atomic force microscopy (AFM) was carried out in tapping mode to characterize the structure of GBP-PVA/SWNTs (Figure 1b). We observe 4 nm globular species (white dots) bound to fibrillar structures of 1 nm average height, as expected. These dimensions are consistent with those of GBP and PVA-wrapped SWNTs (Figure 1c and d). From a collection of such AFM images and optical spectroscopy, we conclude that the majority of complexes consist of a single SWNT with GBP attached to the sidewall. Binding of GBP to cPVA/SWNT was further confirmed by gel electrophoresis, Bradford assay, infrared spectroscopy, and fluorescence spectroscopy (Figures S4–S7).

The excitation–emission profile of GBP-PVA/SWNTs was measured (Figure 2a), showing expected fluorescence peaks originating from three nanotube species, (8,3), (6,5), and (7,5). We conclude that cPVA itself has little effect on nanotube fluorescence and that the SWNTs are individually suspended. Emission spectra of GBP-PVA/SWNTs were also measured in the presence of glucose (Figure 2b) demonstrating an approximately uniform decrease. The peaks at 973, 1001, and 1041 nm are assigned to the (8,3), (6,5), and (7,5) nanotubes; while the peak at 986 nm is attributed to the 2-phonon G′ Raman peak typical of graphene structures.[9] The response is found to be highly selective to glucose, as expected (Figure 2c) since GBP is known to have a high selectivity toward glucose over fructose and mannose. We verified that the mechanism is an exciton quenching after photoabsorption, as the absorption spectrum remains unchanged under the same conditions (Figure S8). GBP-PVA/SWNT conjugates were deposited on a glass substrate and each nanotube was imaged as a bright near-IR pixel cluster that allowed for independent monitoring. Figure 2d exhibits the integrated intensity trace for a single GBP-PVA/SWNT conjugate in the presence of glucose, added at time 120 s. The fluorescence of

[*] Prof. H. Yoon,[+] Dr. J.-H. Ahn,[+] Dr. P. W. Barone, Dr. K. Yum, R. Sharma, A. A. Boghossian, Dr. J.-H. Han, Prof. M. S. Strano
Department of Chemical Engineering
Massachusetts Institute of Technology
77 Massachusetts Avenue, Cambridge, MA 02139 (USA)
Fax: (+1) 617-253-8723
E-mail: strano@mit.edu
Prof. H. Yoon[+]
Department of Polymer and Fiber System Engineering
Chonnam National University
77 Yongbong-ro, Buk-gu, Gwangju 500-757 (South Korea)
[+] These authors contributed equally to this work.

[**] This work was funded by the MIT Deshpande Center for Technological Innovation and a Beckman Young Investigator award for M.S.S.

Supporting information for this article is available on the WWW under http://dx.doi.org/10.1002/anie.201006167.

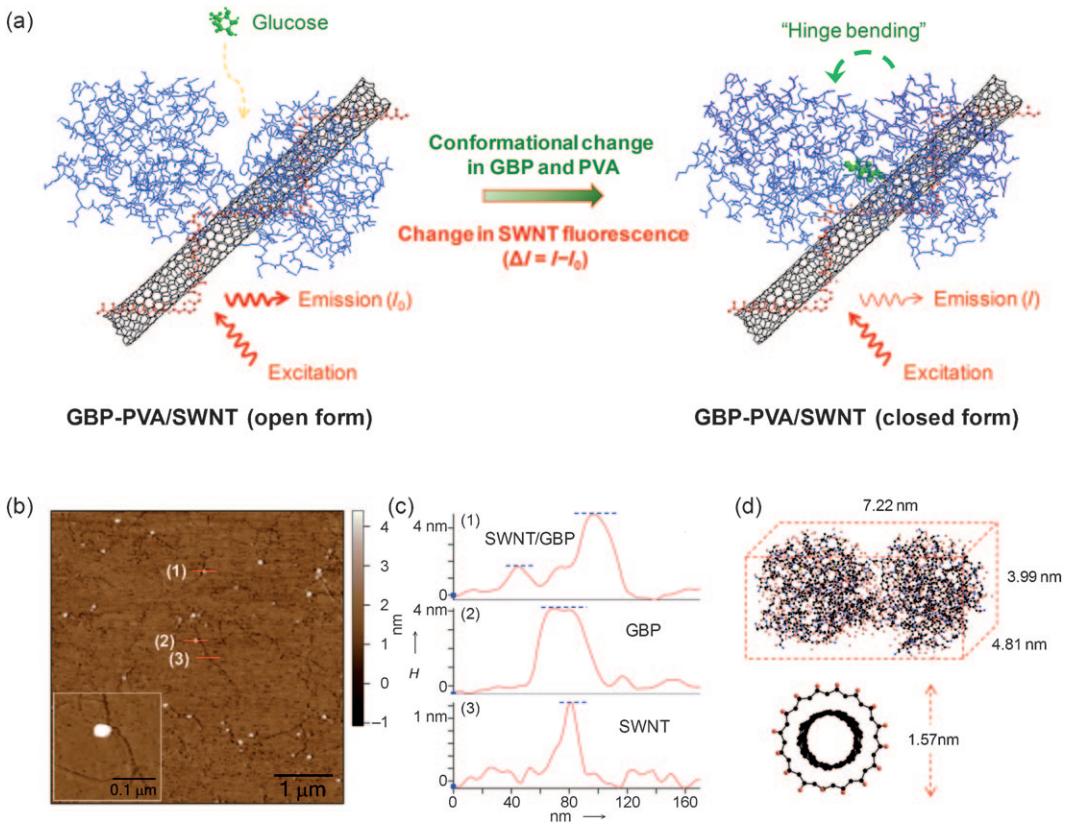

Figure 1. a) Glucose recognition in the GBP-PVA/SWNT conjugate. The difference in the angle between the two structural domains is max. 36°, which arises from torsion angle changes in a three-segment hinge. b) AFM image (left bottom inset: a high magnification image) of GBP-PVA/SWNTs. c) Height information obtained from the AFM image: 1) SWNT and GBP; 2) GBP; 3) SWNT. d) The dimensions of GBP (above, perspective view) and PVA/SWNT (bottom, cross-sectional view) calculated from the minimum-energy configuration.

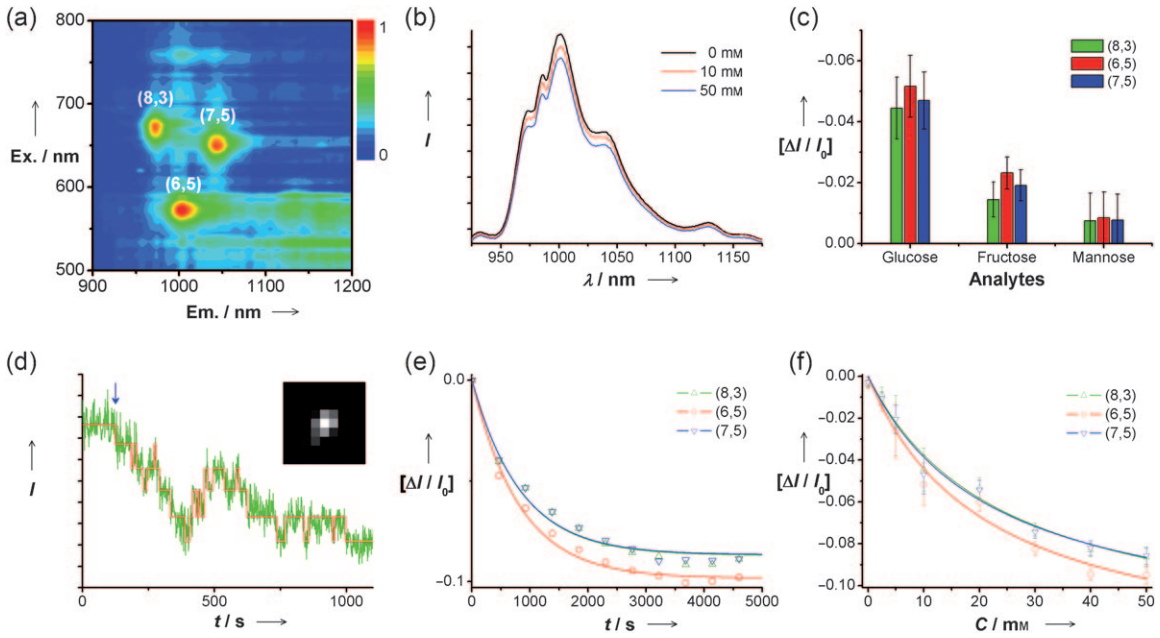

Figure 2. a) Fluorescence profile (excitation vs. emission) of GBP-PVA/SWNTs: the intensity was normalized with the maximum. b) Typical fluorescence spectra of GBP-cPVA/SWNTs before and after glucose introduction ($\lambda_{exc} = 785$ nm). c) Histogram showing the selectivity of GBP-cPVA/SWNTs (at 10 mM sugar). d) NIR fluorescence image (inset, each pixel is 0.5×0.5 μm) and spatially integrated intensity trace for single GBP-PVA/SWNT conjugate recorded in the presence of 10 mM glucose ($\lambda_{exc} = 658$ nm). The blue arrow indicates the addition of glucose. Intensity variations (green) were fitted by a hidden Markov model (red). e) Real-time responses of GBP-PVA/SWNTs upon addition of 50 mM glucose ($\lambda_{exc} = 785$ nm). f) Calibration curves for GBP-PVA/SWNTs. The experimental and calculated data are plotted by symbols and lines, respectively.

the single protein–nanotube conjugate shows quantized blinking associated with stochastic quenching of excitons from adsorption of a quenching entity. In this case, these fluctuations correspond to quenched and dequenched states caused by the GBP, as demonstrated previously for H_2O_2.[10] This result clearly demonstrates that the quenching mechanism in response to glucose involves a single nanotube, and an aggregation step, which is consistent with the above observations.

Changes in the emission from GBP-PVA/SWNTs were systematically investigated at different concentrations of glucose to evaluate the effective affinity towards glucose and the dynamics of actuation. The emission intensity could be monitored consistently over a long observation time (>60 h) due to the photostability of SWNT. Figure 2e describes typical transient responses of GBP-PVA/SWNTs upon glucose addition. The emission intensity decreases before reaching equilibrium over a range of glucose concentrations (2.5 to 50 mM). A calibration curve can be generated from this equilibrium quenching response (Figure 2f) and generally demonstrated linear behavior at low concentrations, with nonlinearity above 10 mM. The responses were similar for all three nanotube species with slightly different sensitivities. No response was observed from a cPVA/SWNT control (absent GBP) (Figure S9). A simple kinetic model describes both the transient and equilibrium GBP-PVA/SWNTs. Since the response is clearly reversible, we formulate a reversible binding mechanism whereby GBP, in response to glucose, actuates the SWNT. Hence, the glucose-GBP binding reaction can be described by:

$$\text{Glucose} + \text{GBP} \rightleftharpoons \text{GBP}^* \tag{1}$$

where GBP* represents the GBP bound with glucose. The rate equation for the above reaction is

$$\frac{d[\text{GBP}^*]}{dt} = k_f[\text{Glucose}][\text{GBP}] - k_r[\text{GBP}^*] \tag{2}$$

where k_f and k_r are constants for [Glucose] ≫ total protein concentration (θ_T). The following equation is derived by integrating Equation (2):

$$[\text{GBP}^*(t)] = \frac{[\text{Glucose}]K_{eq}\theta_T\left\{1 - e^{-\left([\text{Glucose}]k_f + \frac{k_r}{K_{eq}}\right)t}\right\}}{1 + [\text{Glucose}]K_{eq}} \tag{3}$$

In this equation, K_{eq} is the equilibrium binding constant for glucose and protein. The [GBP*(t)] directly affects the fluorescence intensity of the SWNT and thus it can be correlated with the change in emission intensity:

$$\frac{\Delta I}{I_0}(t) = -A\frac{[\text{GBP}^*(t)]}{\theta_T} \tag{4}$$

Here, A is a proportionality factor scaling the response. In the case of $t \rightarrow \infty$ (steady state), K_{eq} and A are calculated from the initial slope of the calibration curve (Table S1). The K_{eq} measures the ability of GBP to bind glucose, which is extrinsically influenced by the open or closed status of the GBP attachment. While suitable covalent immobilization of GBP makes it more stable, excessive covalent bonding can lead to the partial degradation and damage of the protein. We note that the K_{eq} values obtained here, which are considerably lower than that of free, untethered GBP (ca. $10^6\,\text{M}^{-1}$), make the GBP-PVA/SWNT suitable for recognizing glucose in the physiological concentration of 2–30 mM. The agreement between the model and experimental data supports the reversible binding mechanism asserted above.

GBP-PVA/SWNTs were encapsulated in a dialysis microcapillary (Figure 3a; 200 μm inner diameter, 13 kDa molecular weight cutoff) to provide more insight into the glucose–

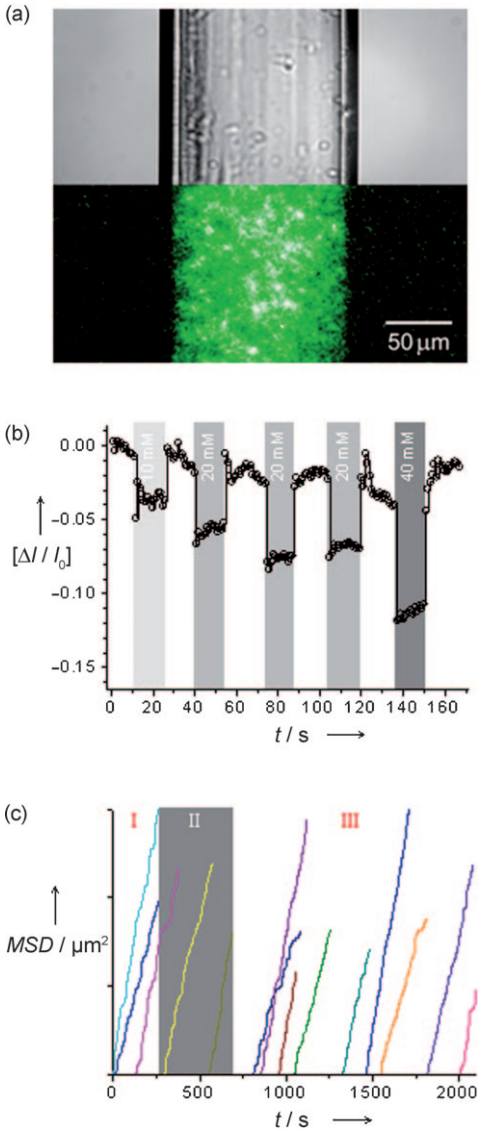

Figure 3. a) Optical (top) and near-infrared fluorescent (bottom) images (λ_{exc} = 658 nm) of the dialysis microcapillary containing GBP-PVA/SWNT solution; for clarity, the fluorescent image was green-colored. b) Response curve of the encapsulated GBP-PVA/SWNTs upon cyclic exposure to glucose (λ_{exc} = 785 nm); the spectra were acquired at 10 s/frame and the (6,5) peak intensity trace was calculated from the collected spectra. The gray-colored region indicates the presence of glucose. c) Examples of MSD curves for three time sections: I) no glucose–GBP interaction; II) glucose–GBP binding; III) glucose–GBP unbinding.

GBP interaction on the PVA/SWNT. The dialysis microcapillary allows diffusion of solutes, which are below the molecular weight cutoff, in and out of the encapsulated solution volume. Figure 3a, bottom shows a NIR fluorescence image of the GBP-PVA/SWNT solution and the surrounding medium which were compartmentalized by the dialysis membrane. The reversibility of the GBP-PVA/SWNT is easily explored in this configuration.[7a,b,d] Upon periodic exposure to glucose, as shown in Figure 3b, the encapsulated GBP-PVA/SWNT had a reversible modulation in fluorescence intensity. This result also confirms the reversibility of the mechanism. In addition, it is important to note that such a reversible response is one of the requirements for continuous monitoring of analytes in certain sensing applications.

Confining the GBP-PVA/SWNT solution into the microcapillary also offered a unique opportunity to explore the diffusion of the nanotube conjugate during the glucose–GBP interaction. Real-time NIR emission from the encapsulated GBP-PVA/SWNT solution was recorded over the course of a one frame-per-second movie, and then a single-particle tracking technique was employed to analyze the individual particle displacements and map out the trajectories. Numerous nanotube trajectories (ca. 80000) were collected to inspect minute dynamic variations involved in the glucose–GBP binding/unbinding events. Each trajectory was numerically analyzed using a standard mean-square displacement (MSD) method to identify its diffusion mode. Figure 3c displays representative plots of MSD versus time for the concerned three conditions during the measurement: I) no glucose–GBP interaction; II) glucose–GBP binding; III) glucose–GBP unbinding. Glucose (50 mM) was added at frame 250 and then removed at frame 650 during the course of the movie. The majority of the MSD curves were linear, indicative of the nanotube conjugates were subject to normal Brownian diffusion in all conditions. This observation implies the following valuable information: 1) there is no interparticle aggregation that can induce a decrease in fluorescence intensity during the measurement; 2) GBP-PVA/SWNTs have high colloidal stability during the microdialysis, which enables continuous monitoring of the reversible binding event. Importantly, these facts support the aforementioned transduction mechanism and the feasibility of microdialysis-based applications again.

In conclusion, we explored the direct coupling of glucose-binding protein (GBP), as a representative periplasmic binding protein (PBP), to near-IR fluorescent SWNT to create a new type of sensor for glucose. The GBP was grafted to a carboxylated polymer non-covalently associated with the nanotube surface such that the hinge-bending response to glucose induces a reversible exciton quenching of the SWNT fluorescence with high selectivity. The transient and equilibrium response are well described using a second order, reversible kinetic model with site conservation that allows calculation of an effective binding constant. The use of PBP as actuators of nanoscale devices may find utility as new types of sensors, micro- and nanofluidic valves, and resonators, and the system demonstrated here specifically may lead to new types of sensor for glucose.[11]

Received: October 1, 2010
Revised: December 13, 2010
Published online: January 18, 2011

Keywords: carbon nanotube · fluorescence · glucose · optical modulation · periplasmic binding protein

[1] a) E. A. Moschou, L. G. Bachas, S. Daunert, S. K. Deo, *Anal. Chem.* **2006**, *78*, 6692; b) M. A. Dwyer, H. W. Hellinga, *Curr. Opin. Struct. Biol.* **2004**, *14*, 495.
[2] a) D. E. Benson, D. W. Conrad, R. M. de Lorimer, S. A. Trammell, H. W. Hellinga, *Science* **2001**, *293*, 1641; b) I. Willner, *Nat. Biotechnol.* **2001**, *19*, 1023.
[3] a) K. M. Ye, J. S. Schultz, *Anal. Chem.* **2003**, *75*, 3451; b) X. D. Ge, L. Tolosa, G. Rao, *Anal. Chem.* **2004**, *76*, 1403; c) V. Scognamiglio, A. Scire, V. Aurilia, M. Staiano, R. Crescenzo, C. Palmucci, E. Bertoli, M. Rossi, F. Tanfani, S. D'Auria, *J. Proteome Res.* **2007**, *6*, 4119; d) J. S. Marvin, H. W. Hellinga, *J. Am. Chem. Soc.* **1998**, *120*, 7; e) Y. Tian, M. J. Cuneo, A. Changela, B. Hocker, L. S. Beese, H. W. Hellinga, *Protein Sci.* **2007**, *16*, 2240; f) T. J. Amiss, D. B. Sherman, C. M. Nycz, S. A. Andaluz, J. B. Pitner, *Protein Sci.* **2007**, *16*, 2775; g) L. L. E. Salins, R. A. Ware, C. M. Ensor, S. Daunert, *Anal. Biochem.* **2001**, *294*, 19; h) L. Tolosa, I. Gryczynski, L. R. Eichhorn, J. D. Dattelbaum, F. N. Castellano, G. Rao, J. R. Lakowicz, *Anal. Biochem.* **1999**, *267*, 114.
[4] N. K. Vyas, M. N. Vyas, F. A. Quiocho, *Nature* **1987**, *327*, 635.
[5] C. L. Careaga, J. Sutherland, J. Sabeti, J. J. Falke, *Biochemistry* **1995**, *34*, 3048.
[6] S. Wray, M. Cope, D. T. Delpy, J. S. Wyatt, E. O. R. Reynolds, *Biochim. Biophys. Acta Bioenerg.* **1988**, *933*, 184.
[7] a) P. W. Barone, S. Baik, D. A. Heller, M. S. Strano, *Nat. Mater.* **2005**, *4*, 86; b) P. W. Barone, R. S. Parker, M. S. Strano, *Anal. Chem.* **2005**, *77*, 7556; c) P. W. Barone, M. S. Strano, *Angew. Chem.* **2006**, *118*, 8318; *Angew. Chem. Int. Ed.* **2006**, *45*, 8138; d) P. W. Barone, H. Yoon, R. Ortiz-Garcia, J. Q. Zhang, J. H. Ahn, J. H. Kim, M. S. Strano, *Acs Nano* **2009**, *3*, 3869; e) P. W. Barone, M. S. Strano, *J. Diabetes Sci. Technol.* **2009**, *3*, 242.
[8] M. J. Borrok, L. L. Kiessling, K. T. Forest, *Protein Sci.* **2007**, *16*, 1032.
[9] J. H. Choi, F. T. Nguyen, P. W. Barone, D. A. Heller, A. E. Moll, D. Patel, S. A. Boppart, M. S. Strano, *Nano Lett.* **2007**, *7*, 861.
[10] a) H. Jin, D. A. Heller, J. H. Kim, M. S. Strano, *Nano Lett.* **2008**, *8*, 4299; b) H. Jin, D. A. Heller, M. Kalbacova, J. H. Kim, J. Q. Zhang, A. A. Boghossian, N. Maheshri, M. S. Strano, *Nat. Nanotechnol.* **2010**, *5*, 302.
[11] a) E. Katz, I. Willner, *Angew. Chem.* **2004**, *116*, 6166; *Angew. Chem. Int. Ed.* **2004**, *43*, 6042; b) K. Teasley Hamorsky, C. M. Ensor, Y. Wei, S. Daunert, *Angew. Chem.* **2008**, *120*, 3778; *Angew. Chem. Int. Ed.* **2008**, *47*, 3718; c) C. B. Mao, A. H. Liu, B. R. Cao, *Angew. Chem.* **2009**, *121*, 6922; *Angew. Chem. Int. Ed.* **2009**, *48*, 6790.

